Ai-xiang Tian*, Ya-li Ning, Huai-ping Ni, Xue Hou, Ru Xiao and Jun Ying

Two new POM-based compounds containing a linear tri-nuclear copper(II) cluster and an infinite copper(II) chain, respectively

Abstract: Using the pendent organic ligand 1-butyl-$1H$-(1,3,4)triazole (btz), two new polyoxometalate (POM)-based compounds, $[Cu_3(btz)_6(H_2O)_4(H_3P_2W_{18}O_{62})_2]\cdot 6H_2O$ (**1**) and $[Cu_2(btz)(tz)(H_2O)_2(SiMo_{12}O_{40})]\cdot 5H_2O$ (**2**) (tz = $1H$-(1,3,4) triazole), have been synthesized under hydrothermal conditions. In compound **1**, three Cu^{II} ions are fused by six btz ligands to form a linear tri-nuclear Cu^{II} cluster, with water as bridging molecules. Two Wells-Dawson anions offer two terminal O atoms to link two apical Cu^{II} atoms of this tri-nuclear cluster. In compound **2**, the btz and tz molecules connect Cu^{II} ions to construct an infinite Cu^{II} chain still with water molecules as bridges. The adjacent chains are linked by one type of POM anions to build a 2D grid-like layer. Considering the long-range coordinative Cu−O bonds, the other types of POM anions connect adjacent layers to form a 3D framework. The electrochemical and photocatalytic properties of compounds **1** and **2** were also studied.

Keywords: electrochemistry; multi-nuclear copper cluster; photocatalytic property; polyoxometalate.

1 Introduction

In recent years, polyoxometalates (POMs), as inorganic metal oxide clusters, have attracted much attention as they own diverse structures [1–3] and applications in the areas of catalysis, magnetism, medicine, and electrochromism [4–6]. Owing to the abundant bridging and terminal oxygen atoms, POMs are always viewed as good inorganic candidates to link metal−organic complexes (MOCs) [7–9], aiming to broaden the scope of structures and property in the POM field. Among various POM types, Wells-Dawson

and Keggin are classical anions and are usually used as inorganic ligands to connect MOCs. A series of Wells-Dawson- and Keggin-based organic−inorganic hybrid compounds have already been synthesized and reported [10, 11]. Thus, using Wells-Dawson and Keggin anions as inorganic ligands is an effective synthetic strategy to coordinate with MOCs, in order to obtain structures with novel topologies and properties.

In POM-based organic−inorganic hybrid compounds, nitrogen donor-containing ligands are commonly used because of their strong coordination ability. In our previous work, we used flexible bis(1,2,4-triazole) ligands as organic moieties, such as 1,3-bis(1,2,4-triazole-1-y1)propane, 1,4-bis(1,2,4-triazole-1-y1)butane, and 1,6-bis(1,2,4-triazole-1-y1)hexane [12–15]. However, the two N donors in this series are discrete, only in favor of forming highly connective and multi-dimensional frameworks. In this work, we change the strategy to choose an isomeric derivative 1,3,4-triazole to construct POM structures, namely 1-butyl-$1H$-(1,3,4)triazole (btz). The two apical N donors of btz can induce multi-nuclear clusters with ease [16]. Though btz contains only one 1,3,4-triazole group, we want to explore whether this simple ligand can still induce novel structures.

Thus, in this work we introduced Wells-Dawson and Keggin anions to the Cu^{II}−btz system, and fortunately, we obtained two POM-based compounds, namely, $[Cu_3(btz)_6(H_2O)_4(H_3P_2W_{18}O_{62})_2]\cdot 6H_2O$ (**1**) and $[Cu_2(btz)(tz)(H_2O)_2(SiMo_{12}O_{40})]\cdot 5H_2O$ (**2**) (tz = $1H$-(1,3,4)triazole). We also studied the electrochemical and photocatalytic properties of these two compounds.

2 Results and discussion

2.1 Structure description of 1 and 2

2.1.1 $[Cu_3(btz)_6(H_2O)_4(H_3P_2W_{18}O_{62})_2]\cdot 6H_2O$ (1)

A single crystal X-ray diffraction study has revealed that compound **1** incorporates three Cu^{II} ions, six btz

Corresponding author: Ai-xiang Tian, Department of Chemistry, Bohai University, Jinzhou, 121013, P.R. China, e-mail: tian@bhu.edu.cn
Ya-li Ning, Huai-ping Ni, Xue Hou, Ru Xiao and Jun Ying: Department of Chemistry, Bohai University, Jinzhou, 121013, P.R. China

ligands, two $[P_2W_{18}O_{62}]^{6-}$ anions (abbreviated to P_2W_{18}), and four coordinated and six crystal water molecules (Fig. 1). The valence sum calculations [17] show that all the W atoms are in the +VI oxidation states and all the Cu atoms are in the +II oxidation states. In order to balance the charge, six protons have been added to the formula.

In compound **1**, there are two crystallographically independent six-coordinated Cu^{II} ions, both showing an octahedral coordination geometry. The Cu1 ion is
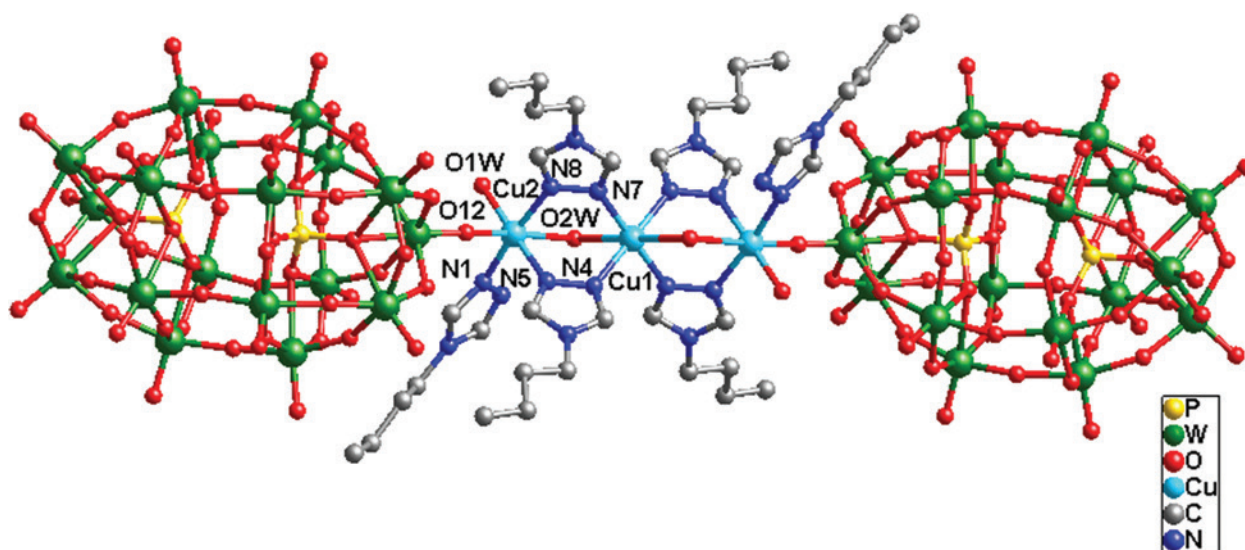

Fig. 1: Ball-and-stick view of the centrosymmetric basic molecular unit of **1**. The hydrogen atoms and crystal water molecules are omitted for clarity.
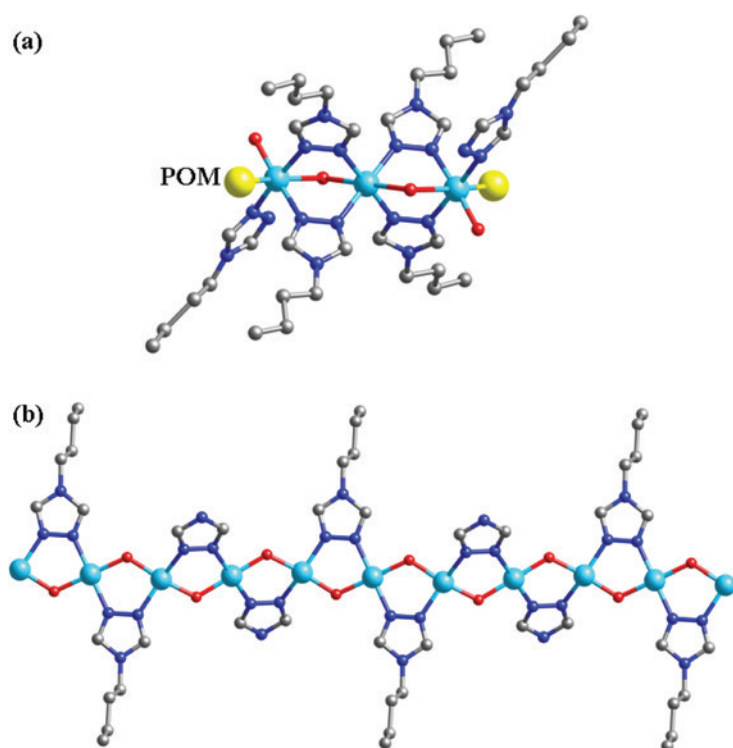

Fig. 2: (a) The linear tri-nuclear cluster in compound **1**. Two P_2W_{18} anions linked Cu^{II} ions are symbolized as yellow spheres; (b) infinite Cu^{II} chain in the crystal structure of **2**.
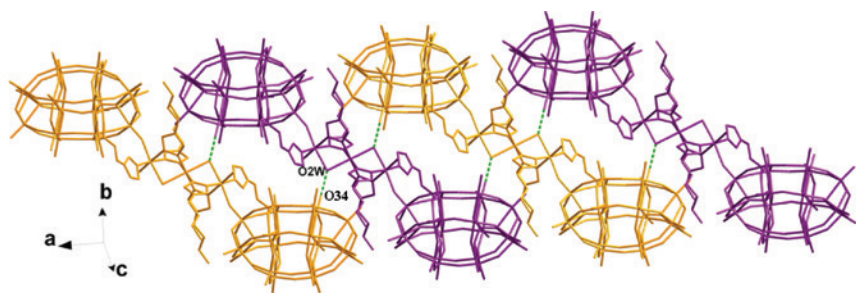
Fig. 3: Supramolecular chain formation in the crystal structure of **1** formed by hydrogen bonding interactions ($O34 \cdots O2W = 2.79$ Å). The molecular units depicted in Fig. 1 are shown here with different colors.

coordinated by four N donors (two N4 and two N7) from four btz ligands and two O2W molecules, whereas the Cu2 ion is coordinated by three N donors (N1, N5, and N8) from three btz ligands, one O12 atom from one P_2W_{18} anion and two water molecules (O1W and O2W). The Cu–N distances are in the range of 1.97(2)–2.007(16) Å, whereas the Cu–O bonds are from 1.93(8) to 2.472(19) Å.

In **1** there exists a linear tri-nuclear Cu^{II} cluster, in which three Cu^{II} ions are fused by six btz ligands. The btz molecule offers its two apical successive N donors to link two Cu^{II} ions. The water molecule O2W acts as a bridging factor to further strengthen this cluster. Two P_2W_{18} anions provide two terminal O12 atoms to connect two apical Cu2 atoms of this tri-nuclear cluster, preventing a dimensional extension (Fig. 2a). Namely, two P_2W_{18} anions cover the linear tri-nuclear Cu^{II} cluster, just like a POM "triple-decker" (Fig. 1). Between adjacent POM "triple-decker", there are several hydrogen bonding interactions inducing a supramolecular 1D chain of **1**, such as $O34 \cdots O2W = 2.73$ Å (Fig. 3).

2.1.2 $[Cu_2(btz)(tz)(H_2O)_2(SiMo_{12}O_{40})]\cdot 5H_2O$ (2)

A single crystal X-ray diffraction analysis has shown that compound **2** consists of two Cu^{II} ions, one btz and one tz ligands, one $[SiMo_{12}O_{40}]^{4-}$ anion (abbreviated to $SiMo_{12}$), two coordinated and five crystal water molecules (Fig. 4). The valence sum calculations [17] show that all the Mo atoms are in the +VI oxidation states and all the Cu atoms are in the +II oxidation states. In compound **2**, the butyl "tail" $-(CH_2)_3CH_3$ of some btz molecules was lost to produce a tz ligand, which also has been observed in previous reports using similar ligands [18, 19]. Thus, in **2**, the btz and tz molecules cooperate to modify the connectivity of the Keggin anions.

In compound **2**, there are three crystallographically independent Cu^{II} ions. The Cu1 ion is four-coordinated by two N5 atoms from two tz ligands and two O1W, showing a square planar coordination geometry. Considering the long-range coordinative Cu2–O28 bonds (2.868 Å), the Cu2 ion is five-coordinated by two N atoms (N2 and N4) from
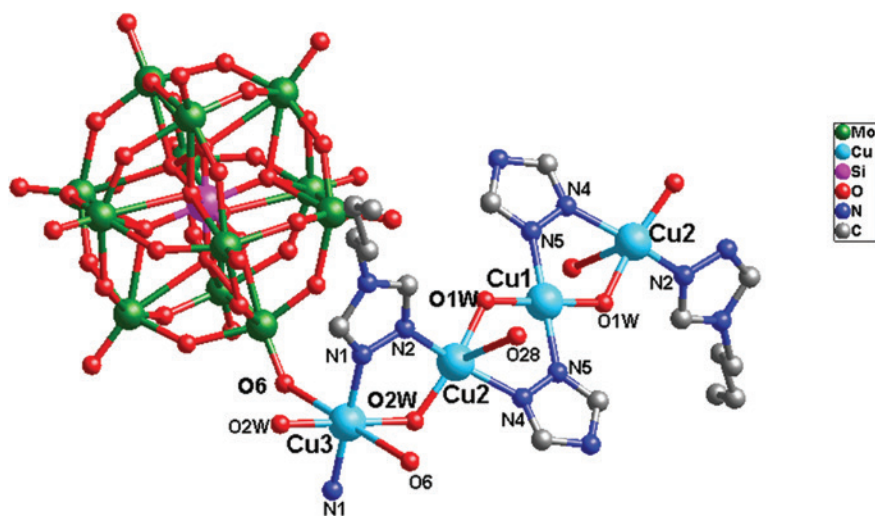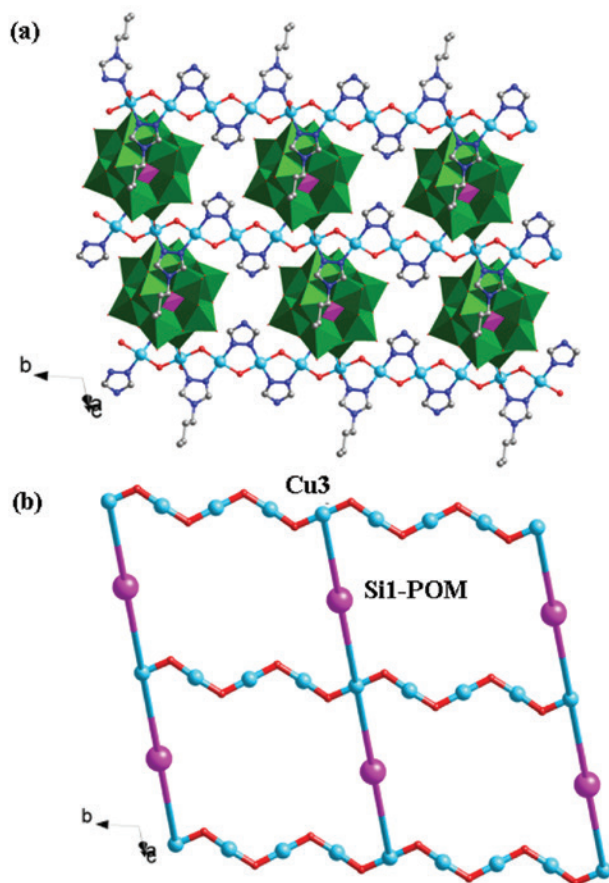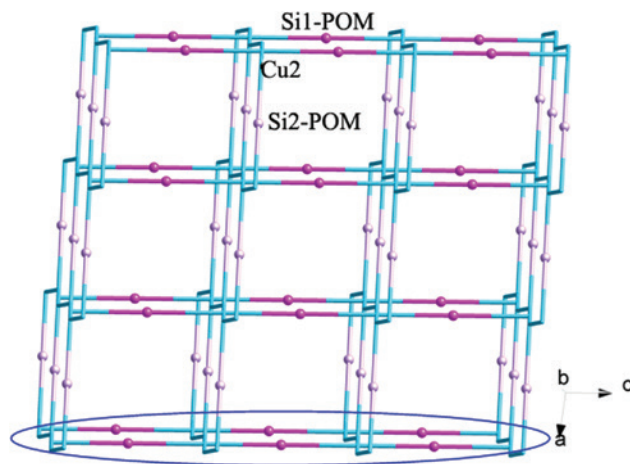

Fig. 4: Ball-and-stick view of the basic molecular unit of **2**. The hydrogen atoms and crystal water molecules are omitted for clarity.

a btz and a tz ligand, respectively, two water molecules (O1W and O2W), and one O28 from one $SiMo_{12}$ anion, exhibiting a distorted tetragonal pyramidal geometry. The Cu3 ion exhibits an octahedral geometry, coordinated by two N1 atoms from two btz ligands, two O6 from two $SiMo_{12}$ anions, and two O2W. The Cu–O bonds are in the range 1.874(8)–2.86(8) Å and the Cu–N bonds are from 1.97(10) to 1.988(9) Å.

Both the btz and tz molecules in **2** provide two successive N atoms to link Cu^{II} ions, inducing an infinite Cu^{II} chain with water molecules as bridges. The btz and tz ligands are attached to this chain up and down alternately (Fig. 2b). In compound **2**, there are two types of $SiMo_{12}$ anions: Si1- and Si2-containing anions. Each Si1-containing anion provides two terminal O6 atoms to fuse Cu3 atoms of adjacent infinite Cu^{II} chains. Thus, a grid-like layer of **2** is formed (Fig. 5). Furthermore, considering the long-range coordinative Cu2–O28 bonds (2.868 Å), the Si2-containing anion can supply two terminal O28 atoms to connect adjacent layers. So a 3D framework is constructed (Fig. 6). In the crystal structure of **2**, there exist large voids

Fig. 6: The 3D framework of compound **2** with Si2-containing anions as linkers.

of about 324 Å³, which may be important for potential applications of this material.

2.2 FT-IR spectra

Figure S1 (Supplementary Information) shows the IR spectra of compounds **1** and **2**. The bands at 1093, 954, 906, and 793 cm^{-1} for **1** are ascribed to the modes of ν(P–O), ν(W–O_d), and ν(W–$O_{b/c}$–W), respectively. In the spectrum of **2**, the characteristic bands at 1089, 968, 906 and 790 cm^{-1} are attributed to ν(Si–O), ν(Mo–O_d), and ν(Mo–$O_{b/c}$–Mo), respectively. Furthermore, the bands in the regions of 1614–1214 cm^{-1} for **1** and 1606–1227 cm^{-1} for **2** are attributed to the btz and tz ligands.

2.3 Photocatalytic activity

Recently, the POM-based compounds have usually been used as photocatalysts to degrade organic dyes [20]. In this work, we also studied the photocatalytic activities of compounds **1** and **2** to degrade methylene blue (MB) and rhodamine B (RhB) solution under UV irradiation. The process of photocatalysis is as follows: 100 mg of compound **1** or **2** was suspended in 0.02 mmol L^{-1} MB or RhB aqueous solution 250 mL. The suspension was magnetically stirred for about 10 min to ensure the equilibrium in the dark. In the continued stirring process, the solution was exposed to UV irradiation from an Hg lamp. Every 30 min, 5.0 mL samples were taken out for analysis by UV/Vis spectroscopy. It can be clearly observed from Fig. 7 that after 120 min the conversions of MB are 45%
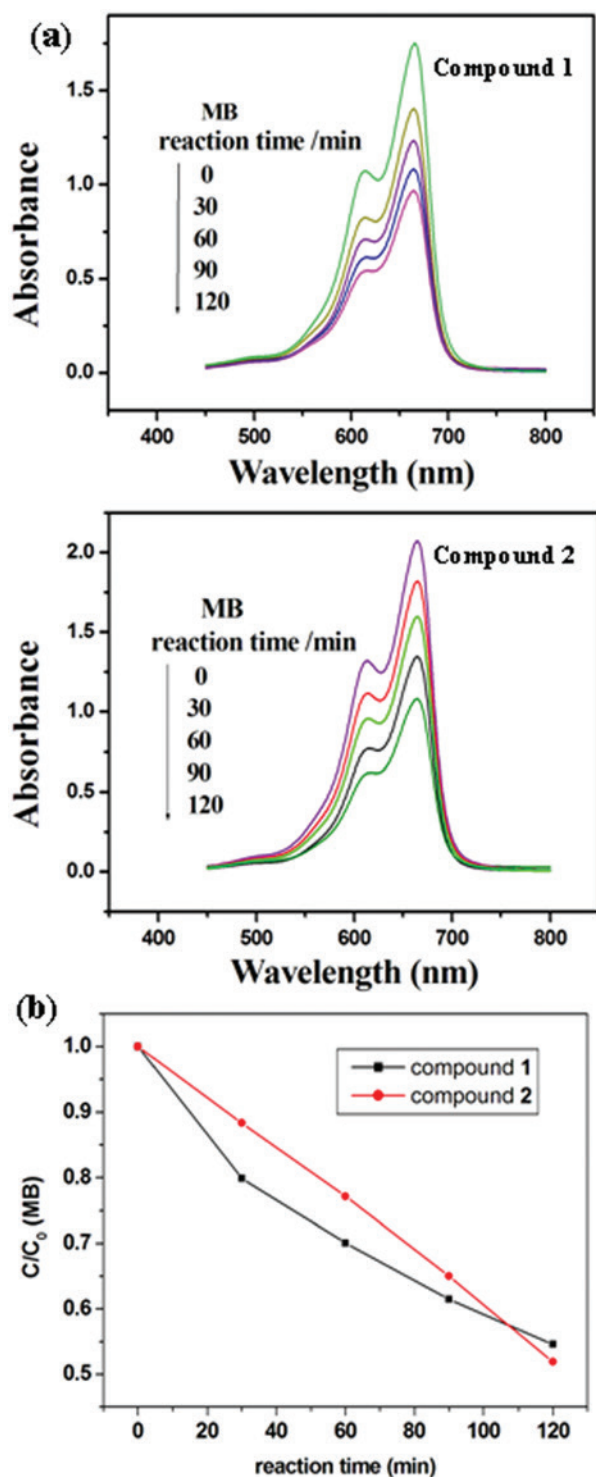

Fig. 5: The grid-like layer (a) and its schematic view (b) of compound **2** with Si1-containing anions as pillars.

Fig. 7: (a) Absorption spectra of the MB solution during the decomposition reaction under UV irradiation with compounds **1** and **2** as catalysts; (b) photocatalytic decomposition rates of the MB solution under UV irradiation with the use of **1** and **2**.
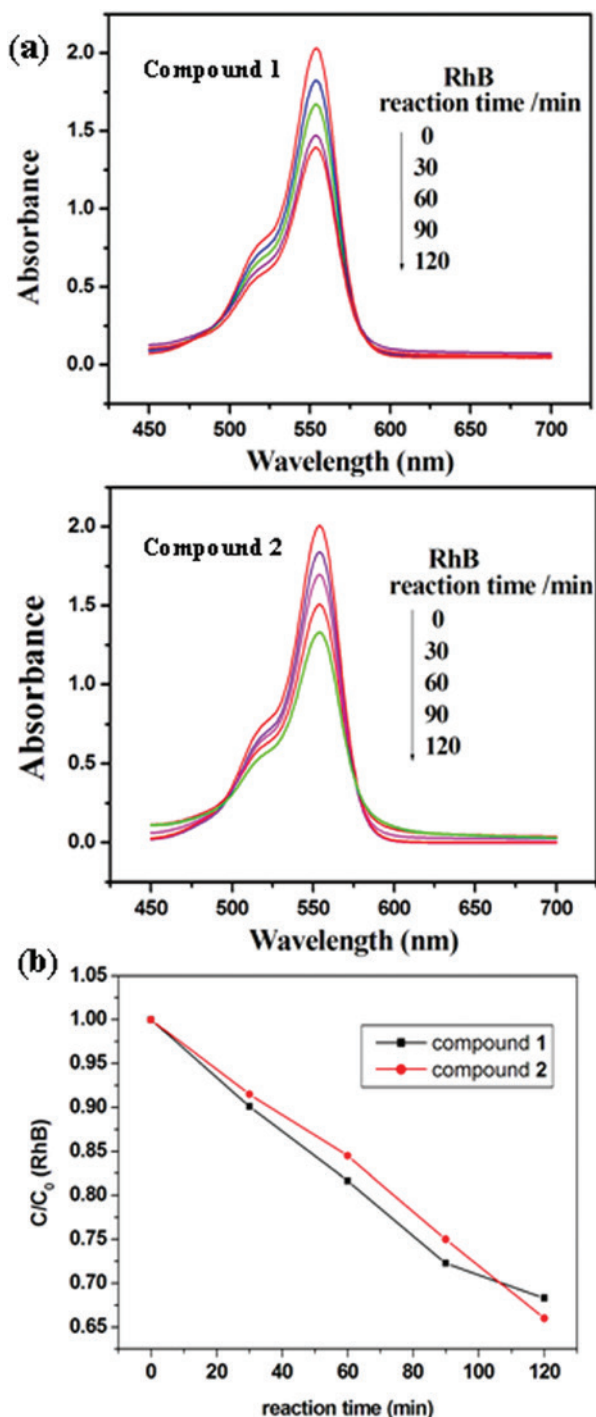

Fig. 8: (a) Absorption spectra of the RhB solution during the decomposition reaction under UV irradiation with compounds **1** and **2** as catalysts; (b) photocatalytic decomposition rates of the RhB solution under UV irradiation with the use of **1** and **2**.

2.4 Voltammetric behavior and electrocatalytic activity

for **1** and 48% for **2**. Figure 8 shows the photocatalytic degradation of RhB and the conversions are 33% for **1** and 35% for **2**.

In this work, we studied the electrochemical properties of **1**- and **2**-CPEs (**1/2** bulk-modified CPE; CPE = carbon

paste electrode). The cyclic voltammograms for **1**- and **2**-CPEs are presented in Fig. 9 for 0.1 м H_2SO_4 + 0.5 м Na_2SO_4 aqueous solutions at different scan rates. In the potential range of +400 to −850 mV for **1**-CPE, three reversible redox peaks II-II′, III-III′, and IV-IV′ are observed, respectively, with the half-wave potentials $E_{1/2} = (E_{pa} + E_{pc})/2$ at −166 (I-I′), −478 (II-II′), −724 (III-III′) mV (scan rate: 80 mV·s⁻¹). These three redox peaks for **1**-CPE should be ascribed to three consecutive two-electron processes of P_2W_{18} [12, 21]. Moreover, there also exists one irreversible anodic peak I′ with the potential of +84 mV, which is assigned to the oxidation of the copper centers [12]. The **2**-CPE shows three reversible redox peaks I-I′, II-II′, and III-III′ in the potential range of +600 to −200 mV, corresponding to three consecutive two-electron processes of $SiMo_{12}$ anions [22]. The half-wave potentials are at +229 (I-I′), +100 (II-II′), and

−89 (III-III′) mV (scan rate: 80 mV·s⁻¹). With the scan rates increasing from 20 to 500 mV·s⁻¹, the peak potentials for **1**- and **2**-CPEs change gradually: the cathodic peak potentials are shifted toward the negative direction, whereas the corresponding anodic peak potentials are shifted to the positive direction.

The electrocatalytic reduction of nitrite by **1**- and **2**-CPEs in 0.1 м H_2SO_4 + 0.5 м Na_2SO_4 aqueous solutions is shown in Fig. 10a. With the addition of nitrite gradually, all the reduced species of P_2W_{18} in **1**-CPE and $SiMo_{12}$ in **2**-CPE present electrocatalytic activity for the reduction of nitrite. We also studied the electrocatalytic reduction of bromate by these CPEs (Fig. 10b). With the addition of bromate, the first redox peak remains almost unchanged, showing that only four- and six-electron-reduced species of P_2W_{18} in **1**-CPE and $SiMo_{12}$ in **2**-CPE present electrocatalytic activity for the reduction of bromate. It was also noted that the six-electron-reduced species presented the largest catalytic activity.
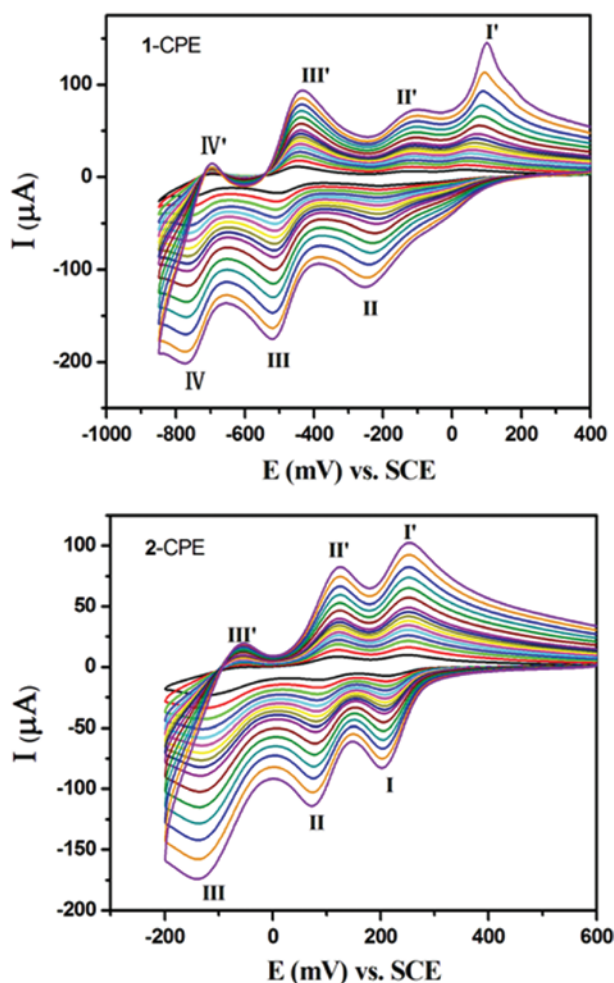
3 Conclusions

In summary, by using btz ligands, we have obtained two new compounds based on Wells-Dawson and Keggin anions, respectively. The two successive N donors of btz induce a linear tri-nuclear Cu^II cluster in **1** and an infinite Cu^II chain in compound **2**. Compound **1** shows a "triple-decker" structure with the tri-nuclear cluster clamped by two Wells-Dawson anions. Compound **2** is a 3D framework with infinite Cu^II chains linked by Keggin anions. Further study on other ligands to build multi-nuclear clusters is underway.

Fig. 9: The cyclic voltammograms of the **1**- and **2**-CPEs in 0.1 м H_2SO_4 + 0.5 м Na_2SO_4 aqueous solution at different scan rates (from inner to outer: 20, 40, 60, 80, 100, 120, 140, 160, 180, 200, 250, 300, 350, 400, 450, and 500 mV·s⁻¹, respectively).

4 Experimental section

4.1 Materials and methods

All reagents and solvents for the syntheses were purchased from commercial sources and used as received without further purification. Elemental analyses (C, H, and N) were carried out with a Perkin-Elmer 2400 CHN elemental analyzer. The FT-IR spectra were taken on Alpha Centaurt FT-IR spectrometer in the 400−4000 cm⁻¹ region (KBr pellets). Electrochemical measurements were performed with a CHI 440 electrochemical workstation. A conventional three-electrode system was used, with modified CPEs as the working electrodes. A saturated calomel electrode was used as a reference
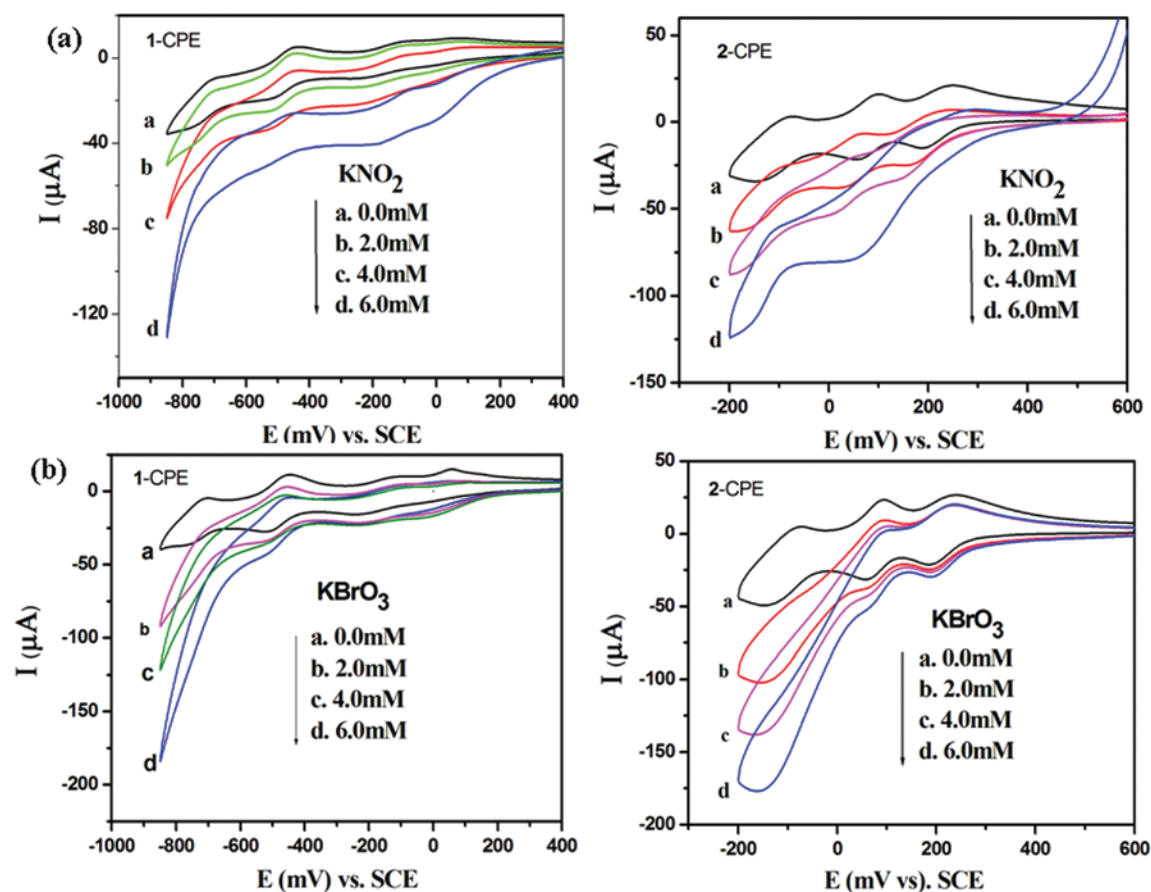
Fig. 10: Cyclic voltammograms of the **1**- and **2**-CPEs in 0.1 M H_2SO_4 + 0.5 M Na_2SO_4 aqueous solution containing KNO_2 (a) and $KBrO_3$ (b). Scan rate: 100 mV·s^{-1}.

electrode, and a Pt wire as a counter electrode. UV/Vis absorption spectra were obtained using an SP-1901 UV/Vis spectrophotometer.

4.2 Synthesis

4.2.1 $[Cu_3(btz)_6(H_2O)_4(H_3P_2W_{18}O_{62})_2]\cdot 6H_2O$ (1)

A mixture of $Cu(CH_3COO)_2\cdot 2H_2O$ (0.064 g, 0.3 mmol), $K_6P_2W_{18}O_{62}$ (0.2 g, 0.04 mmol), and btz (0.031 g, 0.25 mmol) was dissolved in 10 mL of distilled water. The pH of the mixture was adjusted with 1 M HCl solution to 4.4 and the solution then sealed into a 20 mL Teflon-lined autoclave. After heating for 3 days at 150°C, the reactor was slowly cooled to room temperature. Green block crystals were filtered and washed with distilled water (40% yield based on W). – Anal. for $C_{36}H_{92}Cu_3N_{18}O_{134}P_4W_{36}$ (9854): calcd. C 4.39, H 0.94, N 2.56; found C 4.28, H 0.85, N 2.45%. – IR data (KBr pellet, cm^{-1}): 3490(s), 3120(w), 1614(s), 1567(w), 1490(w), 1454(w), 1397(m), 1254(w), 1214(m), 1151(w), 1093(m), 954(m), 906(s), 793(s), 638(w).

4.2.2 $[Cu_2(btz)(tz)(H_2O)_2(SiMo_{12}O_{40})]\cdot 5H_2O$ (2)

Compound **2** was synthesized similarly to **1**, except for using $H_4SiMo_{12}O_{40}\cdot 12H_2O$ (0.41 g, 0.2 mmol) in place of $K_6P_2W_{18}O_{62}$. Blue block crystals were filtered and washed with distilled water (30% yield based on Mo). – Anal. for $C_8H_{27}Cu_2N_6O_{47}SiMo_{12}$ (2265): calcd. C 4.24, H 1.19, N 3.71; found: C 4.35, H 0.88, N 3.74%. – IR (solid KBr pellet, cm^{-1}): 3526(m), 3124(w), 1606(s), 1557(w), 1495(w), 1468(w), 1409(w), 1348(w), 1284(m), 1227(m), 1190(m), 1089(s), 968(s), 906(s), 790(s), 633(w).

4.3 X-ray crystallographic study

X-ray intensity data for compounds **1** and **2** were collected on a Bruker Smart Apex CCD diffractometer with

graphite-monochromatized MoK_α radiation ($\lambda = 0.71073$ Å) at 293 K. The structures were solved by Direct Methods and refined on F^2 by full-matrix least-squares methods using the Shelxtl package [23, 24]. All the hydrogen atoms attached to carbon atoms were generated geometrically. In compound **2**, the five water molecules were highly disordered and could not be modeled properly. As a consequence, the SQUEEZE routine of Platon [25–27] was applied to remove the contributions of the solvent molecules to the scattering power. The reported refinements are of the guest-free structures using the structure factors produced by SQUEEZE [27]. Table 1 shows a summary of the crystallographic data and structure determinations. Selected bond lengths and angles are listed in Table S1 (Supplementary information).

CCDC 1474765 (**1**) and 1474766 (**2**) contain the supplementary crystallographic data for this paper. These data can be obtained free of charge from The Cambridge Crystallographic Data Centre *via* www.ccdc.cam.ac.uk/data_request/cif.

4.4 Preparation of compounds 1 and 2 bulk-modified CPEs

Compound **1** bulk-modified CPE (**1**-CPE) was used as the working electrode, which was prepared as the following process: 90 mg of graphite powder and 8 mg of **1** were mixed and ground together by an agate mortar and pestle to achieve a uniform mixture. Then 0.1 mL of Nujol was added with stirring. The homogenized mixture was packed into a glass tube with a 1.5 mm inner diameter. The tube surface was wiped with weighing paper. Electrical contact was established with a copper rod through the back of the electrode. A **2**-CPE was made with compound **2** in a similar manner.

5 Supplementary information

The IR spectra and selected bond distances and angles for compounds **1** and **2** are given as Supplementary Information available online (http://dx.doi.org/10.15.15/znb-2016-0115).

Table 1: Crystal data and numbers pertinent to data collection and structure refinement of **1** and **2**.

Compound	1	2
Empirical formula	$C_{36}H_{92}Cu_3N_{18}O_{134}P_4W_{36}$	$C_8H_{27}Cu_2N_6O_{47}SiMo_{12}$
Formula weight, M_r	9854	2265
Temperature, K	293(2)	293(2)
Crystal system	Monoclinic	Triclinic
Space group	$P2_1/n$	$P\bar{1}$
a, Å	15.129(2)	12.8614(7)
b, Å	21.003(3)	13.0548(8)
c, Å	23.080(3)	14.7859(8)
α, deg	90	97.359(1)
β, deg	97.897(3)	97.339(1)
γ, deg	90	102.717(1)
V, Å^3	7264.3(19)	2370.3(2)
Z	2	2
$D_{calcd.}$, g·cm^{-3}	4.44	3.04
μ, mm^{-1}	29.0	4.1
$F(000)$, e	8582	2030
θ range, deg	1.52–25	1.41–28.32
Refs. measured	40 719	17 662
Refs. unique/R_{int}	12 779/0.0962	11 805/0.0202
Ref. parameters	952	709
Final $R1^a$/$wR2^b$ [$I > 2\sigma(I)$]	0.0532/0.1100	0.0694/0.1499
Final $R1^a$/$wR2^b$ (all data)	0.0965/0.1206	0.0901/0.1606
GoF (F^2)^c	1.026	0.928
$\Delta\rho_{fin}$ (max/min), e Å^{-3}	3.85/−2.69	3.82/−4.03

$^a R1 = \Sigma ||F_o| - |F_c||/\Sigma |F_o|$.
$^b wR2 = [\Sigma w(F_o^2 - F_c^2)^2/\Sigma w(F_o^2)^2]^{1/2}$, $w = [\sigma^2(F_o^2) + (AP)^2 + BP]^{-1}$, where $P = (\text{Max}(F_o^2, 0) + 2F_c^2)/3$.
$^c \text{GoF} = S = [\Sigma w(F_o^2 - F_c^2)^2/(n_{obs} - n_{param})]^{1/2}$.

References

[1] R. Yu, X. F. Kuang, X. Y. Wu, C. Z. Lu, J. P. Donahue, *Coord. Chem. Rev.* **2009**, *253*, 2872.

[2] D. Lachkar, D. Vilona, E. Dumont, M. Lelli, E. Lacôte, *Angew. Chem. Int. Ed.* **2016**, *55*, 5961.

[3] H. L. Li, Y. J. Liu, R. Zhang, L. J. Chen, J. W. Zhao, G. Y. Yang, *Inorg. Chem.* **2016**, *55*, 3881.

[4] J. J. Walsh, A. M. Bond, R. J. Forster, T. E. Keyes, *Coord. Chem. Rev.* **2016**, *306*, 217.

[5] A. Kumar, M. Devi, N. Mamidi, K. E. Gonsalves, C. P. Pradeep, *Chem. Eur. J.* **2015**, *21*, 18557.

[6] S. J. Li, S. M. Liu, S. X. Liu, Y. W. Liu, Q. Tang, Z. Shi, S. X. Ouyang, J. H. Ye, *J. Am. Chem. Soc.* **2012**, *134*, 19716.

[7] J. Zhou, J. W. Zhao, Q. Wei, J. Zhang, G. Y. Yang, *J. Am. Chem. Soc.* **2014**, *136*, 5065.

[8] J. Lü, J. X. Lin, X. L. Zhao, R. Cao, *Chem. Comm.* **2012**, *48*, 669.

[9] A. B. Lysenko, G. A. Senchyk, L. V. Lukashuk, K. V. Domasevitch, M. Handke, J. Lincke, H. Krautscheid, E. B. Rusanov, K. W. Krämer, S. Decurtins, S. X. Liu, *Inorg. Chem.* **2016**, *55*, 239.

[10] M. L. Qi, K. Yu, Z. H. Su, C. X. Wang, C. M. Wang, B. B. Zhou, C. C. Zhu, *Dalton Trans.* **2013**, *42*, 7586.

[11] J. Ying, Y. L. Ning, X. Hou, R. Xiao, J. W. Zhang, A. X. Tian, *Z. Naturforsch.* **2014**, *69b*, 871.

[12] A. X. Tian, J. Ying, J. Peng, J. Q. Sha, Z. G. Han, J. F. Ma, Z. M. Su, N. H. Hu, H. Q. Jia, *Inorg. Chem.* **2008**, *47*, 3274.

[13] A. X. Tian, J. Ying, J. Peng, J. Q. Sha, H. J. Pang, P. P. Zhang, Y. Chen, M. Zhu, Z. M. Su, *Inorg. Chem.* **2009**, *48*, 100.

[14] A. X. Tian, J. Ying, J. Peng, J. Q. Sha, H. J. Pang, P. P. Zhang, Y. Chen, M. Zhu, Z. M. Su, *Cryst. Growth. Des.* **2008**, *8*, 3717.

[15] A. X. Tian, H. P. Ni, Y. Tian, X. B. Ji, G. C. Liu, J. Ying, *Inorg. Chem. Commun.* **2016**, *68*, 50.

[16] A. X. Tian, Y. Yang, J. Ying, N. Li, X. L. Lin, J. W. Zhang, X. L. Wang, *Dalton Trans.* **2014**, *43*, 8405.

[17] I. D. Brown, D. Altermatt, *Acta Crystallogr.* **1985**, *B41*, 244.

[18] A. X. Tian, Y. L. Ning, J. Ying, X. Hou, T. J. Li, X. L. Wang, *Dalton Trans.* **2015**, *44*, 386.

[19] A. X. Tian, Y. L. Ning, J. Ying, J. W. Zhang, X. Hou, T. J. Li, X. L. Wang, *Dalton Trans.* **2015**, *44*, 10499.

[20] Y. Q. Chen, G. R. Li, Y. K. Qu, Y. H. Zhang, K. H. He, Q. Gao, X. H. Bu, *Cryst. Growth. Des.* **2013**, *13*, 901.

[21] P. P. Zhang, J. Peng, H. J. Pang, J. Q. Sha, M. Zhu, D. D. Wang, M. G. Liu, *CrystEngComm*. **2011**, *13*, 3832.

[22] M. Sadakane, E. Steckhan, *Chem. Rev*. **1998**, *98*, 219.

[23] G. M. Sheldrick, Sʜᴇʟxᴛʟ, Bruker Analytical X-ray Instruments Inc., Madison, WI (USA) **2001**.

[24] G. M. Sheldrick, *Acta Crystallogr*. **2008**, *A64*, 112.

[25] A. L. Spek, Pʟᴀᴛᴏɴ, A Multipurpose Crystallographic Tool, Utrecht University, Utrecht (The Netherlands) **2010**.

[26] A. L. Spek, *Acta Crystallogr*. **2009**, *D65*, 148.

[27] A. L. Spek, *Acta Crystallogr*. **2015**, *C71*, 9.